Cell Stem Cell
Article

Functional Maturation of hPSC-Derived Forebrain Interneurons Requires an Extended Timeline and Mimics Human Neural Development

Cory R. Nicholas,[1,7] Jiadong Chen,[1,7] Yunshuo Tang,[2] Derek G. Southwell,[2,8] Nadine Chalmers,[1] Daniel Vogt,[3] Christine M. Arnold,[2] Ying-Jiun J. Chen,[3] Edouard G. Stanley,[5,6] Andrew G. Elefanty,[5,6] Yoshiki Sasai,[4] Arturo Alvarez-Buylla,[2] John L.R. Rubenstein,[3] and Arnold R. Kriegstein[1,*]
[1]The Eli and Edythe Broad Center of Regeneration Medicine and Stem Cell Research, Department of Neurology
[2]The Eli and Edythe Broad Center of Regeneration Medicine and Stem Cell Research, Department of Neurological Surgery
[3]Department of Psychiatry and the Nina Ireland Laboratory of Developmental Neurobiology
University of California, San Francisco, San Francisco, CA 94158, USA
[4]Organogenesis and Neurogenesis Group, RIKEN Center for Developmental Biology, Kobe 650-0047, Japan
[5]The Murdoch Children's Research Institute, The Royal Children's Hospital, Parkville, Victoria 3052, Australia
[6]Monash Immunology and Stem Cell Laboratories (MISCL), Monash University, Clayton, Victoria 3800, Australia
[7]These authors contributed equally to this work
[8]Present address: Department of Neurosurgery, Stanford University, Stanford, CA 94305, USA
*Correspondence: kriegsteina@stemcell.ucsf.edu
http://dx.doi.org/10.1016/j.stem.2013.04.005

SUMMARY

Directed differentiation from human pluripotent stem cells (hPSCs) has seen significant progress in recent years. However, most differentiated populations exhibit immature properties of an early embryonic stage, raising concerns about their ability to model and treat disease. Here, we report the directed differentiation of hPSCs into medial ganglionic eminence (MGE)-like progenitors and their maturation into forebrain type interneurons. We find that early-stage progenitors progress via a radial glial-like stem cell enriched in the human fetal brain. Both in vitro and posttransplantation into the rodent cortex, the MGE-like cells develop into GABAergic interneuron subtypes with mature physiological properties along a prolonged intrinsic timeline of up to 7 months, mimicking endogenous human neural development. MGE-derived cortical interneuron deficiencies are implicated in a broad range of neurodevelopmental and degenerative disorders, highlighting the importance of these results for modeling human neural development and disease.

INTRODUCTION

In contrast to excitatory (glutamatergic) cortical pyramidal neurons that project long distances, inhibitory (GABAergic) cortical interneurons make local synapses and are essential for maintaining the balanced activity of neural circuits (Markram et al., 2004). Most cortical interneurons are born in the MGE of the developing ventral telencephalon midgestation and, subsequently, undergo tangential migration into the neocortex (Anderson et al., 2001; Wichterle et al., 2001). During late gestational to early postnatal stages, nascent interneuron precursors gradually develop into extremely diverse subtypes of GABAergic interneurons that can be classified by their morphology, expression of neuropeptide- and/or calcium-binding protein subtype markers, and intrinsic physiological membrane properties (Figure 1A) (Markram et al., 2004). Interneuron maturation occurs with the progressive acquisition of features that include increasing cell size and branching of processes, expression of subtype markers, formation of GABAergic synapses, ability to fire high-frequency trains of action potentials (APs), and development of more mature electrophysiological properties (Le Magueresse and Monyer, 2013).

Deficiencies in subtypes of interneurons, and the resulting excitatory-inhibitory imbalances, have been associated with many neuro-developmental and -degenerative disorders, such as epilepsy, schizophrenia, autism, and Alzheimer's disease (Chao et al., 2010; Cheah et al., 2012; Cobos et al., 2005; Fazzari et al., 2010; Verret et al., 2012). The ability to derive mature subtypes of human interneurons from patients could provide a basis for studying the etiology as well as the potential therapeutic targets for diseases of interneuron dysfunction.

In this study, we investigate the maturation of human pluripotent stem cell (hPSC)-, including human embryonic stem cell (hESC)- and human induced pluripotent stem cell (hiPSC)-, derived MGE-like progenitors into functional GABAergic interneuron subtypes. Prior studies have reported the differentiation of various neural lineages from hPSCs, including ventral forebrain-like precursor cells (Elkabetz et al., 2008; Goulburn et al., 2011; Kim et al., 2011; Li et al., 2009; Ma et al., 2012; Watanabe et al., 2007). However, aside from two recent reports studying cortical-like excitatory projection neurons (Espuny-Camacho et al., 2013; Shi et al., 2012), there has been little focus on the maturation of hPSC-derived progenitor cells into functional neuronal subtypes that develop advanced physiological properties. Here, we use cell morphology, global gene expression profiling, subtype marker expression, and electrophysiological analyses to demonstrate mature features of interneuron

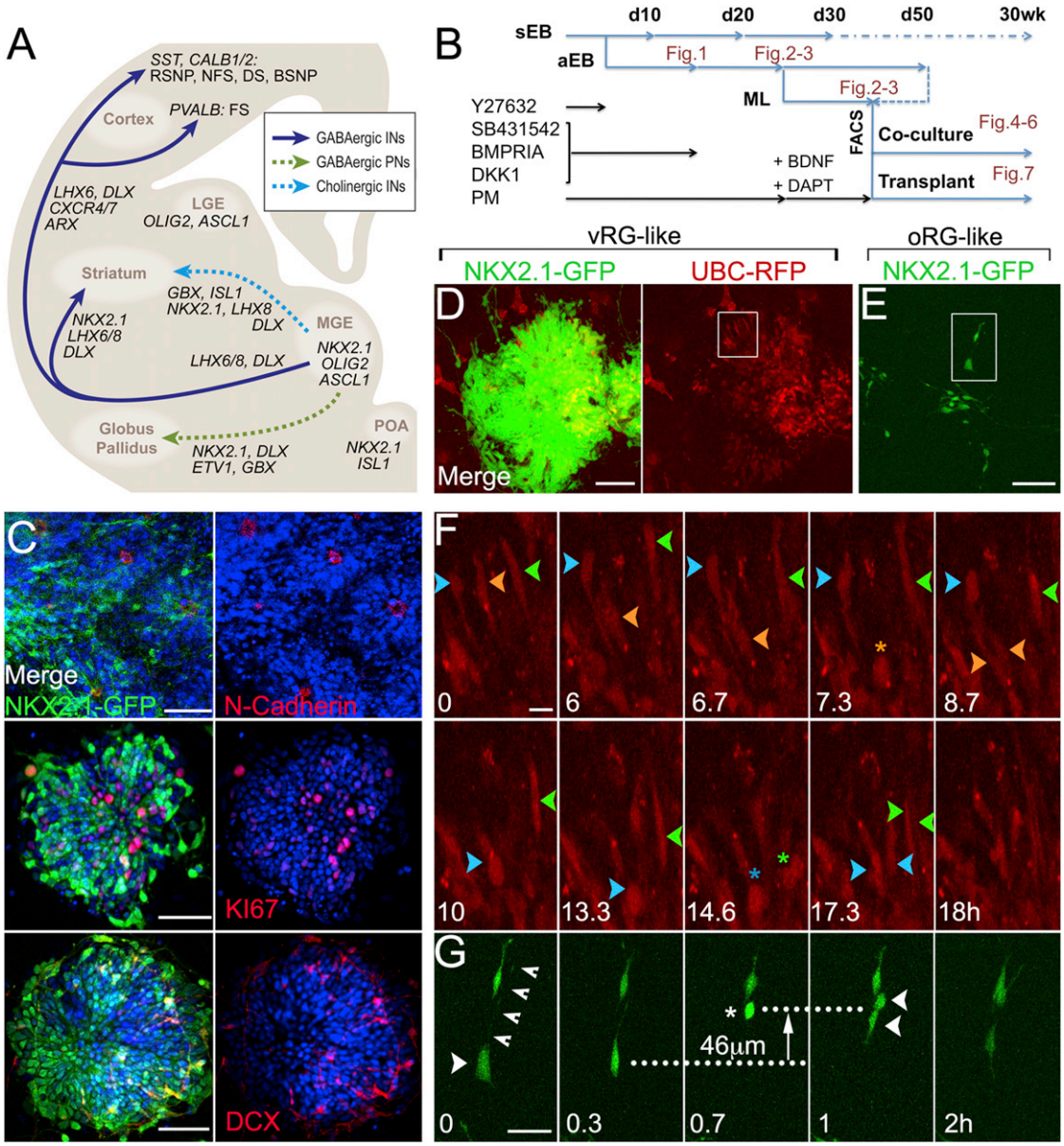

Figure 1. hPSC-Derived MGE-like Progenitors Exhibited VZ and SVZ Radial Glial-like Stem Cell Divisions

(A) A schematic of neuronal lineages emanating from the MGE, their gene expression profiles, and major cortical interneuron subtypes. INs, interneurons; PNs, projection neurons; FS, fast-spiking; RSNP, regular-spiking nonpyramidal; NFS, non-fast-spiking; DS, delayed-spiking; BSNP, burst-spiking nonpyramidal.

(B) An outline of the B27+5F method and its corresponding figures. sEB, suspension embryoid body; aEB, adherent embryoid body; ML, monolayer; FACS, fluorescence-activated cell sorting; Y27632, Rho-associated kinase (ROCK) inhibitor; SB431542I, inhibitor of the TGFβ1 activin receptor-like kinases; BMPRIA, bone morphogenetic protein receptor 1a Fc chimera; DKK1, Dickkopf homolog 1; PM, Purmorphamine; BDNF, brain-derived neurotrophic factor; DAPT, inhibitor of γ-secretase.

See also Supplemental Experimental Procedures, Figures S1–S3, and Table S1.

(C) Day 14 *NKX2.1*-GFP expression and a panel of markers in red shown merged and separate. Markers include N-Cadherin, KI67, and DCX. DAPI expression is shown in blue. The scale bar represents 50 μm.

(D) A cluster of rosettes with RFP fluorescence alone or merged with *NKX2.1*-GFP. The scale bar represents 100 μm.

(E) *NKX2.1*-GFP-expressing cells outside of the clusters. The scale bar represents 100 μm.

(F) Time-lapse imaging series of boxed region (D) showing three RFP+ cells (blue, orange, and green arrowheads) that displayed vRG-like INM behavior; translocation toward the rosette lumen and division (star) with a vertical cleavage plane. Time: hours. The scale bar represents 20 μm.

See also Movie S1.

(G) Time-lapse series of boxed region (E). A GFP+ cell with characteristic unipolar morphology (white arrowhead and smaller arrowheads to mark fiber) exhibited oRG-like MST behavior; translocation toward the fiber (46 μm) and division (star) with a horizontal cleavage plane. Time is shown in hours. The scale bar represents 50 μm.

See also Movies S2 and S3.

subtypes during their protracted functional maturation from hPSCs. We find that mature hPSC-derived interneurons fire subtype-specific trains of APs, receive synaptic inputs, generate GABAergic-exclusive synaptic output, and functionally integrate postinjection into the rodent cortex. Moreover, we find that stem-cell-derived interneurons acquire these mature features according to an intrinsic developmental timeline shared with endogenous human interneuron subtypes.

RESULTS

hPSC-Derived Telencephalic MGE-like Identity

To facilitate the identification of hPSC-derived MGE-like cells, we used the HES-3 hESC line (HES-3 *NKX2.1*$^{GFP/w}$) with a GFP knockin construct inserted into the second exon of *NKX2.1* (Goulburn et al., 2011). NKX2.1 expression marks ventral forebrain-specific identity in the developing nervous system, including the telencephalic MGE, preoptic area (POA), septum, and diencephalic hypothalamus. In combination with dual SMAD (SB431542 and BMPRIA-Fc), ROCK (Y27632), and WNT (DKK1) inhibition (Chambers et al., 2009; Li et al., 2009; Watanabe et al., 2007), we found that optimization of early SHH pathway activation (purmorphamine) and B-27 supplementation enabled highly efficient and reproducible ventral forebrain-like differentiation from hESCs. The average *NKX2.1*-GFP+ efficiency on day 20–30 postdifferentiation was 74.9% ± 2.1% (n = 25 independent differentiation experiments). We also found that additional hESC lines, including cGMP-matched ESI-017, ESI-035, ESI-051, ESI-053 (BioTime), and H9 (WiCell), and an adult melanocyte-derived hiPSC line differentiated into NKX2.1+ MGE-like cells at a similar efficiency. The optimized B27 + five factor (B27+5F) method is outlined in Figure 1B and described in detail in Figure S1 and the Supplemental Experimental Procedures (available online).

To determine the regional identity of the *NKX2.1*-GFP+ cells, we performed a 50 day time course of suspension embryoid body (sEB) differentiation and immunostaining analysis for markers of forebrain development (Figures S2 and S3). We detected robust *NKX2.1*-GFP expression by day 10 of differentiation that colocalized with NKX2.1 protein and was expressed throughout the time course. In contrast, PAX6, a marker of dorsal telencephalic neural progenitors, was not detected. Telencephalon marker FOXG1 was found in most cells by day 20 and remained highly expressed. In opposition to this trend, NKX2.2 expression, a marker of hypothalamus and more ventrocaudal regions, was primarily only expressed between days 10–20. Interestingly, the transient appearance of NKX2.2+ ventral diencephalic-like cells may represent a stage of early forebrain development prior to the emergence of the FOXG1+ ventral telencephalon (Shimamura and Rubenstein, 1997). Additional ventral telencephalic progenitor markers OLIG2 and ASCL1 (MASH1) were induced by day 20–30. By day 30, sEBs expressed the migratory neuronal marker doublecortin (DCX) and the neurotransmitter GABA. We did not detect the hypothalamic marker RAX or cholinergic neuron marker CHAT. Therefore, the hPSC-derived *NKX2.1*-GFP+ cells represented a telencephalic MGE-like GABAergic neuronal lineage. A summary of marker expression during sEB culture is provided in Table S1.

hPSC-Derived MGE-like Progenitors Exhibited VZ and SVZ Radial Glial-like Stem Cell Behaviors

A defining feature of embryonic neural development is the acquisition of apicobasal polarity and the production of radial glial neural stem cells (Kriegstein and Götz, 2003). There is evidence that neuroepithelial progenitors in hESC-derived neural rosettes represent apicobasal-like polarity (Elkabetz et al., 2008). When sEBs were plated en bloc on days 4–7, the adherent EBs (aEBs) flattened and revealed the organization of *NKX2.1*-GFP+ cells in rosette structures. N-cadherin expression was restricted to the rosette lumenal surface, confirming polarity, and was consistent with localization to radial glial-end feet on the apical ventricular surface in the embryonic brain (Figure 1C). Mitotic marker KI67 was expressed in many cells, particularly in those near the rosette lumen (Figure 1C). In contrast, neuronal markers ASCL1 (data not shown) and DCX (Figure 1C) were detected away from the lumen.

Rosettes were labeled with RFP (*ubiquitin C* promoter-RFP [*UbC*-RFP] virus) and were monitored by live time-lapse imaging. We detected *NKX2.1*-GFP+ and *UbC*-RFP+ cells in rosette structures displaying ventricular zone (VZ) radial glia (vRG)-like interkinetic nuclear migration (INM) behavior prior to division (Figures 1D and 1F). VRG-like cell bodies translocated toward the rosette lumen and divided with a vertical cleavage plane (parallel to the fiber) (Movie S1). Interestingly, daughter cells appeared to extend radial fibers, resembling the symmetrical divisions attributed to embryonic vRGs that divide with a vertical cleavage plane.

Next, we investigated whether recently described (Fietz et al., 2010; Hansen et al., 2010) human-enriched outer subventricular zone (OSVZ) radial glial (oRG)-like cells were present in our cultures. We focused on *NKX2.1*-GFP+ cells with unipolar fibers located away from the rosette clusters (Figures 1E and 1G). We discovered GFP+ oRG-like cells displaying mitotic somal translocation (MST) prior to division. These cell bodies translocated toward the unipolar fiber and divided with a horizontal cleavage plane (perpendicular to the fiber) (Movies S2 and S3). In summary, hPSC-derived MGE-like progenitors recapitulated VZ and human-enriched OSVZ radial glial-like stem cell behaviors.

hPSC-Derived MGE-like Progenitors Generated GABAergic Interneurons

Furthermore, we explored the identity and fate of the hPSC-derived MGE-like cultures. Immunostaining analysis was conducted on day 25 aEBs and day 35 dissociated monolayer (ML) cultures, and forebrain marker expression was quantified on day 35 (Figure 2). At both stages, *NKX2.1*-GFP expression was specific to cells expressing endogenous NKX2.1 protein (91.3% ± 1.7%). On day 25, FOXG1 and OLIG2 were expressed in most of the *NKX2.1*-GFP+ cells (Figure 2B). By day 35, most GFP+ cells continued to express FOXG1 (81.5% ± 3.6%) but had downregulated OLIG2 (6.8% ± 3%). Conversely, the majority of GFP+ cells on day 35 upregulated ASCL1 (79.9% ± 6.5%) and DLX2 (79.8% ± 3.7%) (Figures 2D and 2E). Given that OLIG2 marks GE progenitors, whereas ASCL1 and DLX2 mark GABAergic neuronal lineages, these results suggested that MGE-like progenitors began to differentiate into GABAergic neurons and were confirmed by the detection of TUJ1 (92% ± 2.4%) and GABA (75.8% ± 2.3%) (Figures 2D and 2E). The interneuron subtype marker calbindin (*CALB1* or CB) was also expressed by

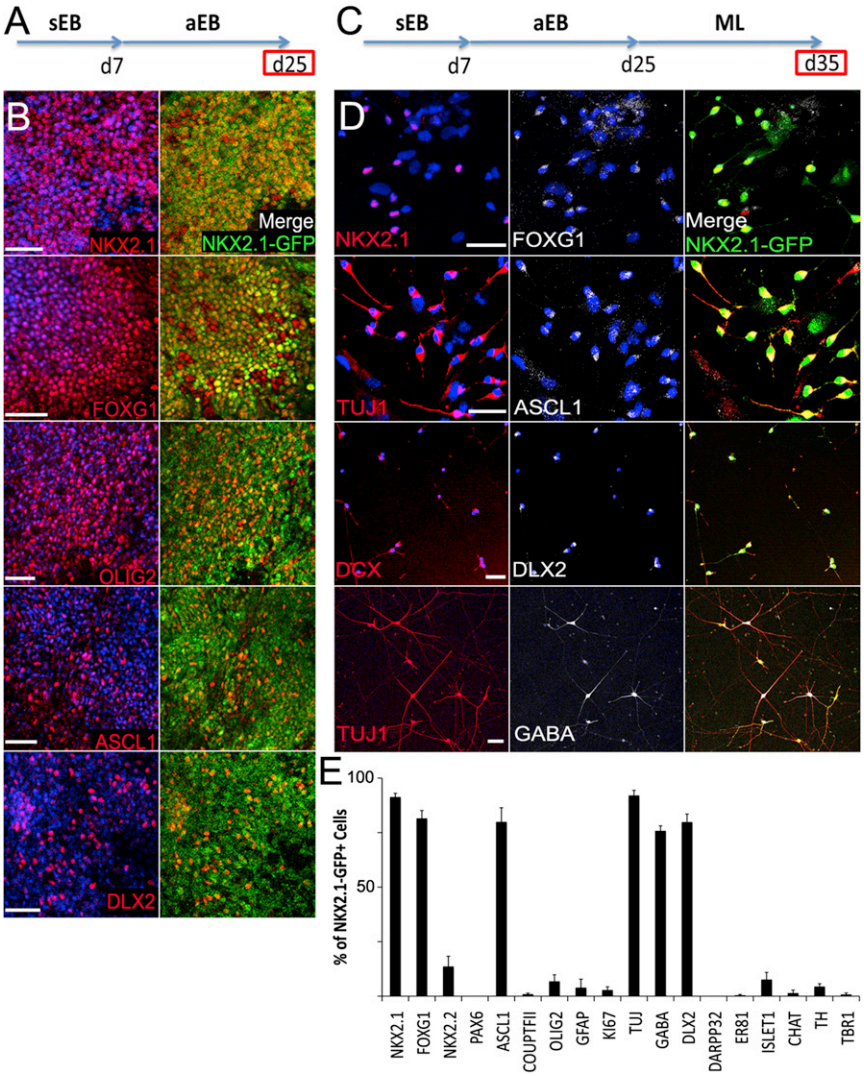

Figure 2. hPSC-Derived MGE-like Progenitors Differentiated into Neurons with Properties of Telencephalic GABAergic Interneurons

(A) aEBs were fixed for immunofluorescence analysis on day 25.

(B) Day 25 MGE-like progenitor cells robustly expressed *NKX2.1*-GFP, NKX2.1, FOXG1, and OLIG2. Some expressed ASCL1 and DLX2. DAPI expression is shown in blue. The scale bar represents 50 μm.

(C) aEBs were dissociated, replated as a ML, and fixed for day 35 immunofluorescence.

(D) Day 35 dissociated cells continued to express *NKX2.1*-GFP, NKX2.1, FOXG1, and upregulated TUJ1, ASCL1, DCX, DLX2, and GABA. DAPI expression is shown in blue. The scale bar represents 50 μm.

(E) A quantification of day 35 immunostaining. The majority of *NKX2.1*-GFP+ cells expressed NKX2.1, FOXG1, ASCL1, TUJ, GABA, and DLX2. Data represented as mean ± SEM.

day 35 (31.1% ± 5.4%), but other interneuron subtype markers calretinin (*CALB2* or CR), somatostatin (*SST*), and parvalbumin (*PVALB* or PV) were not yet detected, suggesting an immature neuronal stage.

A minority of GFP+ cells expressed NKX2.2 (13.6% ± 4.7%), the neural progenitor and glial cell marker GFAP (3.9% ± 3.9%), mitotic marker KI67 (2.8% ± 1.5%), LGE- and POA-enriched ISLET1 (7.6% ± 3.3%), or dopaminergic neuron marker TH (4.4% ± 1.3%). Virtually none of the GFP+ cells expressed PAX6, the CGE and dorsal MGE marker COUPTFII, striatal medium spiny neuron marker DARPP32, globus pallidus projection neuron marker ER81 (*ETV1*), CHAT, or glutamatergic neocortical projection neuron marker TBR1 (Figure 2E). On the basis of these results, hPSC-derived MGE-like progenitors differentiated into predominantly postmitotic GABAergic interneuron precursor cells by day 35.

hPSC-Derived *NKX2.1*-GFP+ Microarray Profiling

We performed microarray profiling to obtain a global transcriptome comparison of undifferentiated hPSCs and FACS-sorted *NKX2.1*-GFP+ populations over a 55 day time course of differentiation (Figure 3A). The percentage of *NKX2.1*-GFP+ cells remained at a high level in dissociated monolayer culture (~81% on d35) or in coculture (~94% of RFP+ cells on d55) (Figure 3B). Dendrogram clustering analysis showed the differentiated GFP+ populations to be more closely related to each other than to undifferentiated hPSCs (Figure S4A). We compared transcript expression for panels of lineage-specific markers and performed quantitative RT-PCR (qRT-PCR) to confirm a subset of the array data (Figures 3 and S4B). Markers of pluripotency were detected only in undifferentiated hPSCs, whereas markers of a neuronal lineage (*HES5*, *TUBB3*, *DCX*, *SYP*, and *SYN1*) increased over time in differentiating GFP+ cells. Markers of glial cells, neural crest, or microglia were not detected. Then, we examined anterior-posterior CNS patterning and detected the expression of primarily anterior CNS markers (*FOXG1*, *SIX3*, and *OTX2*).

Then, we investigated markers that identify subregions of the forebrain. Aside from the temporary expression of *NKX2.2*, markers of diencephalic hypothalamus were not robustly expressed (Figure S4C). Also, dorsal excitatory neuronal lineage markers were not detected (Figure S4D). Instead, ventral telencephalic GABAergic neuronal lineage markers (*ASCL1*, *DLX1*, and *DLX5*) were expressed along with MGE markers (*NKX2.1*, *LHX6*, *LHX8*, and *CXCR7*), and their expression intensities generally increased over time (Figures 3F and 3H). GABAergic markers (*GAD1*, *SLC32A1*, and *SLC6A1*) were found, but glutamatergic or cholinergic neuronal markers were not expressed (Figure 3G). Of the interneuron subtype markers, robust *SST* transcript and weaker *CALB1/2* signals were detected by day 55 (Figure 3H). These results suggested that GFP+ cells were of a principally telencephalic MGE-like GABAergic interneuron lineage.

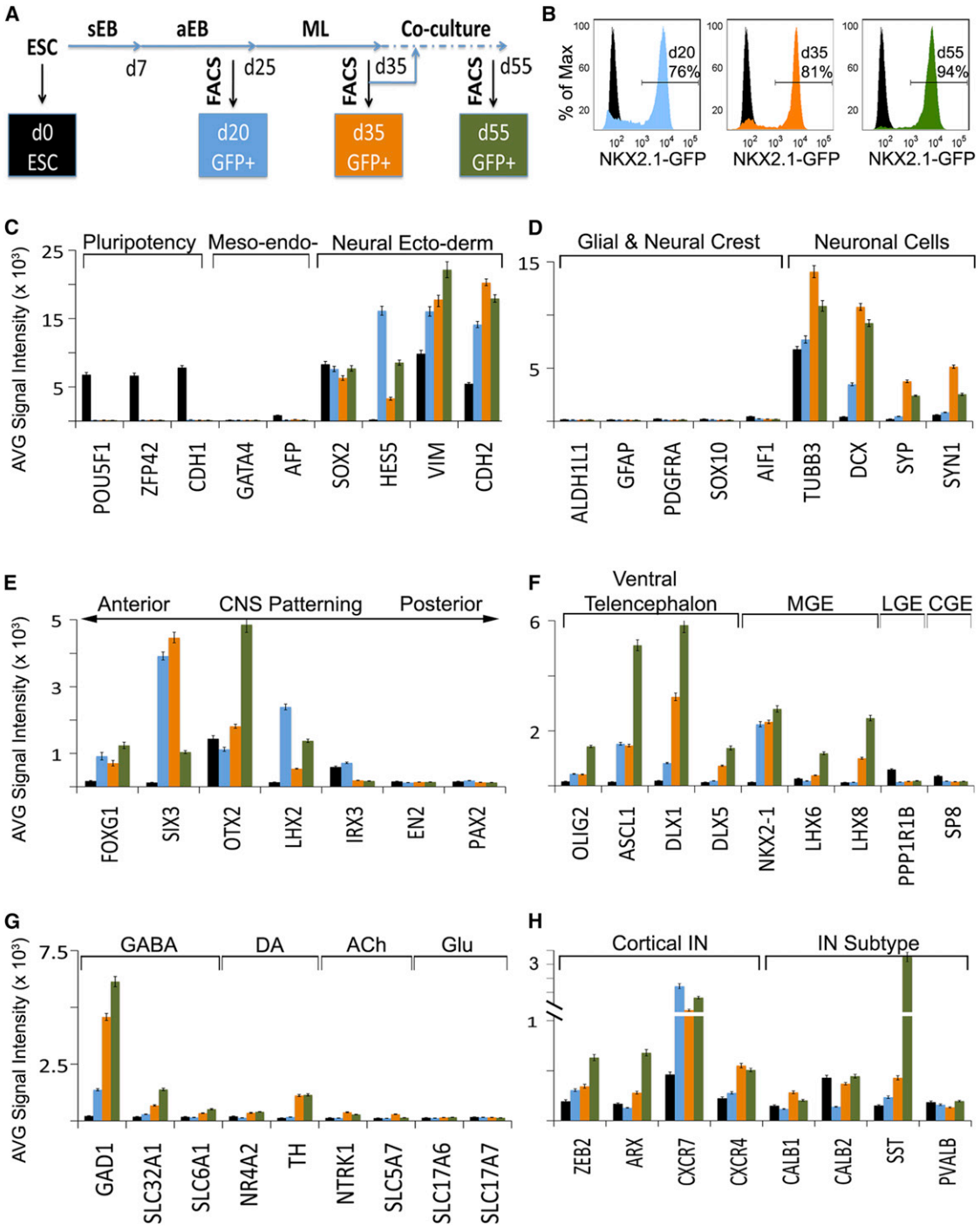

Figure 3. Microarray Gene Expression Profiling of hPSC-Derived MGE-like *NKX2.1*-GFP+ Cell Populations

(A) A schematic and legend for the microarray data. Undifferentiated hPSCs are shown in black, FACS-sorted GFP+ cells from day 20 aEBs are shown in blue, day 35 ML cultures are shown in orange, and GFP+ cells from d35 cocultured to day 55 are shown in green.

(B) Representative FACS histogram analysis of each differentiation stage and undifferentiated hPSC controls (black).

(C–H) Average transcript hybridization signal intensities for marker panels. IN, interneuron; DA, dopaminergic; ACh, cholinergic; Glu, glutamatergic. Data are represented as mean ± SEM.

See also Figure S4.

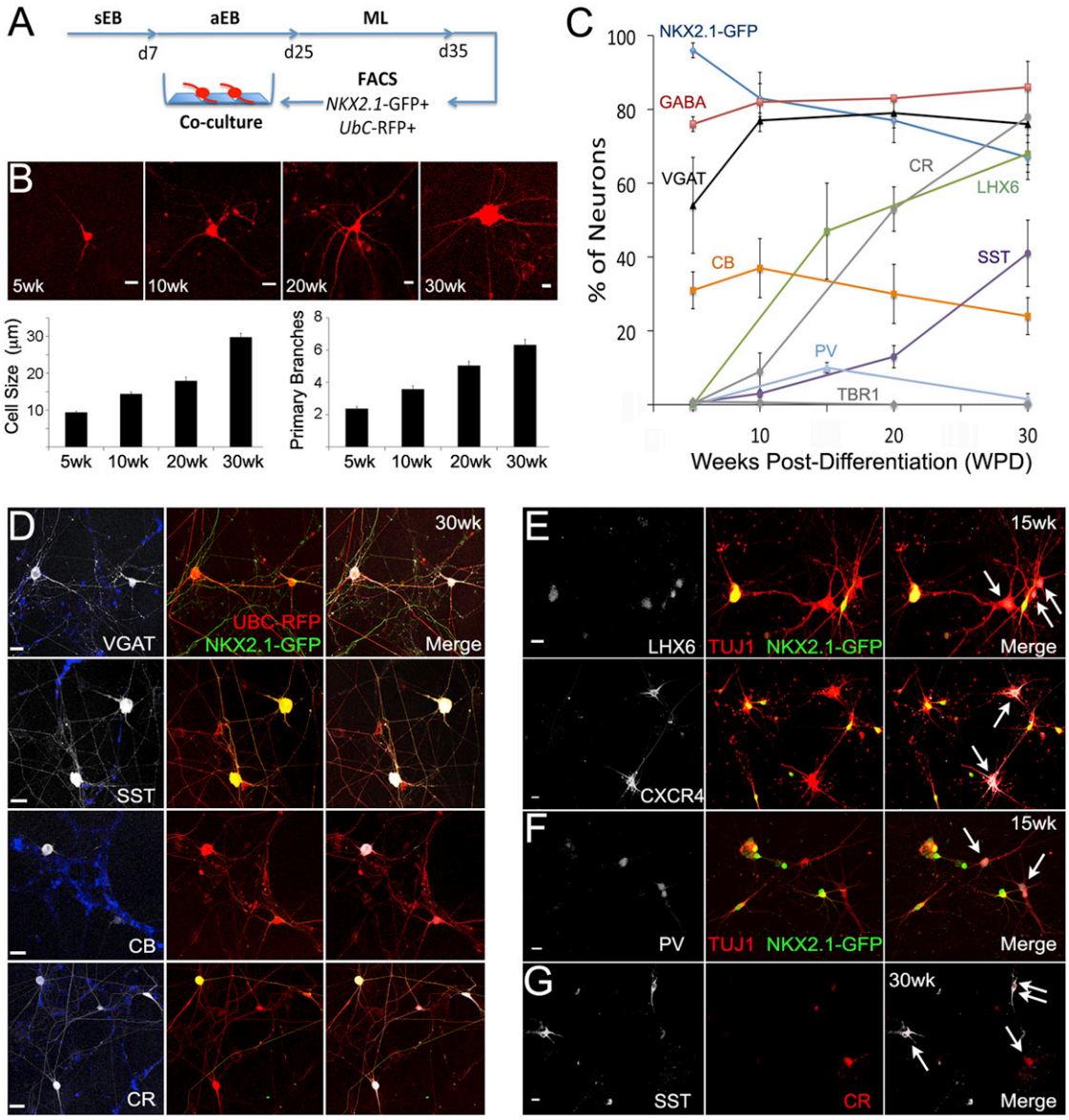

Figure 4. Maturation of hPSC-Derived GABAergic Interneurons Expressing Subtype Markers

(A) Shown are dissociated ML cultures infected with *UbC*-RFP lentivirus, FACS-sorted on day 35 for GFP+ and RFP+ cells, and cocultured.

(B) RFP+ neurons increased in size and dendritic complexity over time. The scale bar represents 20 μm. Cell somal size (μm) and number of primary branches are quantified as mean ± SEM.

(C) Quantification of immunostaining analyses over 30 WPD. Data are represented as mean ± SEM.

(D) Immunostaining of 30 WPD cultures showing highly branched RFP+ neurons that expressed VGAT, SST, CB, and CR. The scale bar represents 50 μm.

(E and F) hPSC-derived TUJ1+ neurons at 15 WPD expressed LHX6, CXCR4, and PV. Some LHX6+, and most CXCR4+ and PV+, neurons downregulated NKX2.1 (arrows), suggesting a cortical-type interneuron lineage. Scale bars represent 20 μm.

(G) Shown is double immunolabeling for SST and CR at 30 WPD. Single positives are indicated with arrows, and double positive are indicated with double arrows. Scale bars represent 20 μm.

See also Figure S5.

Protracted Maturation of hPSC-Derived MGE-like Cells into GABAergic Interneurons Expressing Subtype Markers

We sought to determine both the mature neuronal subtypes generated by the *NKX2.1*-GFP+ MGE-like precursors and their developmental timeline. In order to study their maturation, day 35 FACS-sorted GFP+ cells were cocultured with cortical glial cells (Figure 4A), and some cells were labeled with *UbC*-RFP virus prior to coculture. Cultures were fixed for analysis along a time course of 30 weeks postdifferentiation (WPD), and interneuron subtype marker expression was quantified. Over time, RFP+ hPSC-derived neurons increased significantly in cell somal size (from 10 to 30 μm by 30 WPD) and displayed more elaborate branching of processes (from 2 to 6 primary

branches by 30 WPD) (Figure 4B, n = 25 cells or more per time point). Most of the neurons expressed GABA (75%–86%) and VGAT (53%–78%) from 5 to 30 WPD (Figures 4C and 4D). Aside from rare cells (11 of 3,110), TBR1 was not expressed.

Similar to cortical interneurons that downregulate NKX2.1 during tangential migration from the MGE to the neocortex (Nóbrega-Pereira et al., 2010), the percentage of reporter *NKX2.1*-GFP+ (Figure 4C) and endogenous NKX2.1+ (data not shown) neurons significantly declined from 5 to 30 WPD (96.1% ± 1.8% to 66.7% ± 6.1%; p = 0.03). Conversely, CXCR4 is expressed in migrating cortical interneurons (Wang et al., 2011) and was also upregulated in a fraction (23%) of the hPSC-derived interneurons (Figure 4E), particularly in neurons that downregulated NKX2.1 (47%). LHX6 is a specific marker of the MGE downstream of NKX2.1 and is required for the specification and maturation of SST and PV interneuron subtypes (Zhao et al., 2008). We detected an increasing percentage of hPSC-derived interneurons that expressed LHX6 over time (68% ± 3% by 30 WPD). LHX6 was expressed in NKX2.1+ and NKX2.1− neurons (Figure 4E), consistent with its endogenous expression in both MGE-derived cortical and striatal interneuron lineages. Therefore, these results suggest a mixed population of cortical (NKX2.1−, CXCR4+, and LHX6+)- and striatal (NKX2.1+, CXCR4−, LHX6+)-type hPSC-MGE-derived interneuron lineages and complement the detection of cortical (*ZEB2* or *Zfhx1b*, *ARX*, and *CXCR4/7*) and striatal (*NKX2.1* and *LHX8*) lineage transcripts (Figures 3F and 3H).

Next, we examined the expression of interneuron subtype markers SST, PV, CB, and CR (Figure 4C and 4D). CB was expressed in neurons throughout the time course (24%–36%). In contrast, the percentage of SST+ and CR+ interneurons increased over time and were significantly upregulated from 10 to 20 WPD (SST: 2.8% ± 1% to 12.8% ± 9%, p = 0.03; CR: 8.8% ± 4.9% to 52.6% ± 6.2%; p = 0.004). By 30 WPD, the percentage of SST+ neurons increased to 40.6% ± 8.6%, and CR+ neurons increased to 77.7% ± 14.9%. NPY+ neurons were scarce (6 of 819 neurons) (data not shown). We found neurons expressing PV at 15 WPD (10% ± 1.4%, Figure 4F); however, only rare PV+ interneurons remained by 30–40 WPD (1.5% ± 1.4%). In addition, we did not detect PV lineage marker KV3.1 (data not shown) or fast-spiking firing properties. Given that the hPSC-derived interneurons predominantly expressed SST and CR subtype markers, we performed costaining to determine whether these were distinct or overlapping populations (Figure 4G). We found that only 3.6% of SST+ or CR+ neurons coexpressed these markers by 15 WPD, but 26.3% of SST+ or CR+ neurons coexpressed the markers by 30 WPD. Thus, hPSC-derived interneurons gradually expressed CB, CR, SST, and CR+SST subtype markers along an extensive time course.

Interestingly, this protracted timeline of differentiation appears similar to endogenous human interneuron subtype development (Fertuzinhos et al., 2009). We confirmed these findings with our own histological analysis of developing human fetal and infant cortex and fetal MGE (Figures S5A and S5B). To further investigate human fetal MGE-derived fates, we dissected and cocultured 18 gestational week (gw) human fetal MGE cells and labeled them with *UbC*-RFP virus. By 12 weeks in culture, RFP+ human fetal MGE cells had matured into CB+, CR+, SST+, and GABA+ neurons, and they did not express TBR1 (Figure S5C). Therefore, hPSC-derived interneuron maturation paralleled the temporal sequence of endogenous human interneuron subtype marker expression.

Maturation of hPSC-Derived Interneuron Subtype Firing Properties

To test whether the hPSC-derived cells were functional neurons, we performed whole-cell patch recordings in order to examine their electrophysiological properties at different WPD (8 WPD, n = 21; 12 WPD, n = 35; 15 WPD, n = 31; 30 WPD, n = 18). We found that AP firing patterns of hPSC-derived neurons were quite immature at 8 WPD, judged by the broad AP half-width of the first AP, small afterhyperpolarization (AHP), reduced AP velocity (dV/dt) in a train of AP firing near threshold, and the inability to fire repetitively upon superthreshold current injection (Figures 5C–5E and 5I). The peak voltage-gated Na^+ and K^+ channel currents increased significantly from 8 to 12 WPD (Figures 5F and 5G), concomitant with a significant decrease in membrane resistance (Rm) (Figure 5I). Most neurons showed more mature repetitive AP firing upon near threshold current injection at 12 and 15 WPD (Figures 5C, S6B, and S6C). By 30 WPD, hPSC-derived neurons exhibited mature AP firing properties with faster and consistent AP velocity near threshold firing (Figure 5C), smaller AP half-width (Figure 5I), and larger AHPs (Figures 5D and 5E) as well as high-frequency repetitive AP firing upon superthreshold current injection (Figures 5C and S6D). We performed postrecording immunostaining analysis on neurobiotin-filled neurons from 30 WPD and found that five out of seven neurons were SST+ (Figure 5B), which was consistent with their nonpyramidal regular spiking firing pattern (Figures 5C and S6D).

Along with more mature AP firing properties, we found corresponding changes in the biophysical properties of hPSC-derived interneurons over time. Neurons at 30 WPD showed a significant increase in membrane capacitance (Cm), more hyperpolarized resting membrane potential (RMP), and a significant decrease in Rm (Figure 5I) that correlated with increased cell-body size and dendritic complexity (Figures 4B and 5A). Consistent with the pace of subtype marker expression, hPSC-derived interneurons demonstrated a slow, 30 week maturation of firing properties.

hPSC-Derived Interneurons Formed Synapses and Generated Functional GABAergic Output

Next, we investigated the synaptic properties of hPSC-derived interneurons cocultured with mouse glial cells. *NKX2.1*-GFP+ neuronal processes colocalized with punctate presynapatic VGAT expression, suggesting the formation of GABAergic synapses (Figure 6A). Spontaneous postsynaptic currents (sPSC) were detected by 8 WPD, and the percentage of neurons receiving sPSCs increased from 33.3% at 8 WPD (n = 12) to 82.1% at 12 WPD (n = 28), along with increased sPSC frequency (Figures 6C and S6G). Furthermore, sPSCs were fully blocked by the $GABA_A$ receptor inhibitor bicuculline methiodide (BMI, 20 μM), indicating functional GABAergic-specific synapse formation (Figure 6B). To confirm that GABAergic neurons were able to send outputs to neighboring neurons, we used optogenetics and transfected half of the cells with *Synapsin* promoter

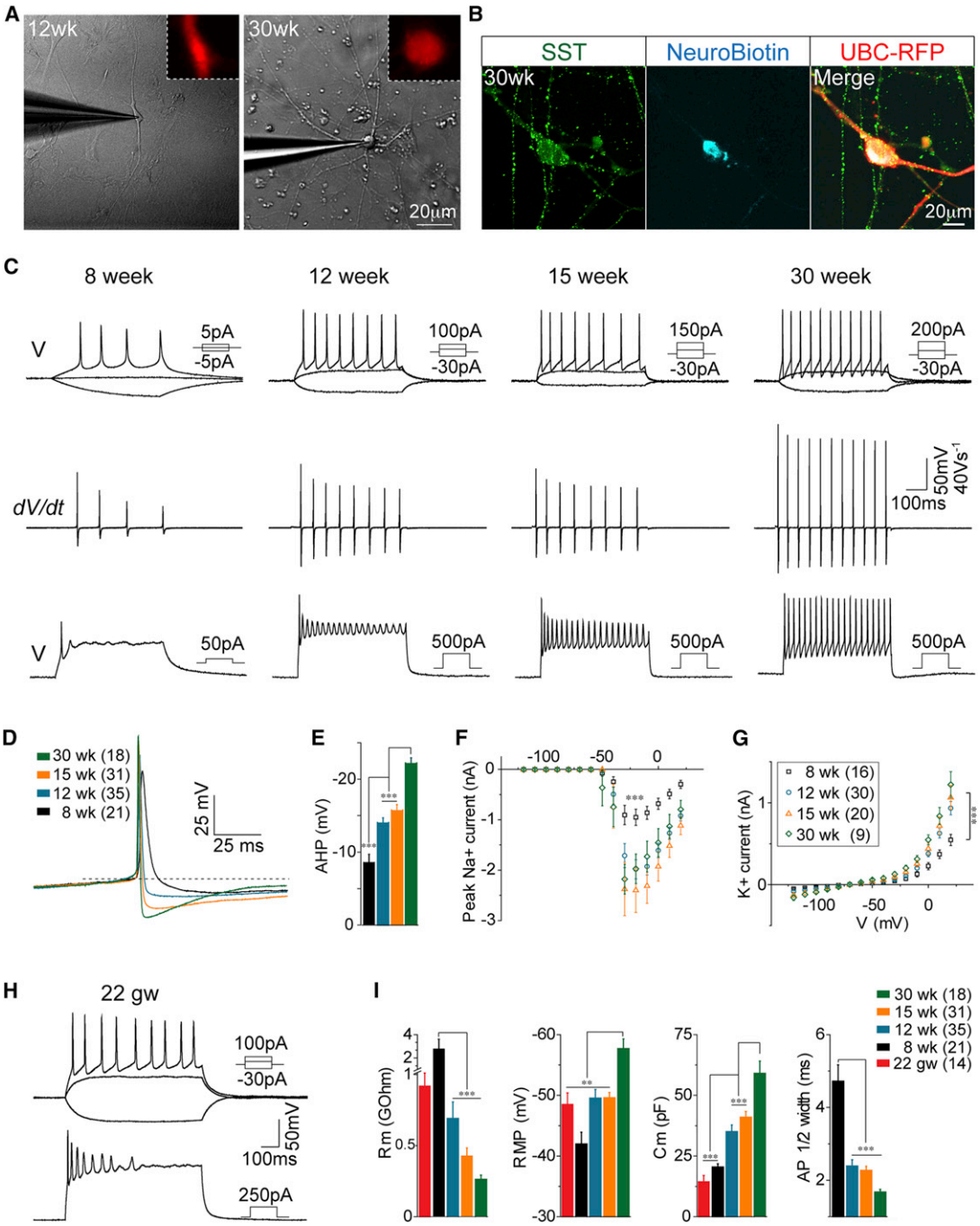

Figure 5. Maturation of hPSC-Derived Interneuron Firing Properties

(A) A DIC image of hPSC-derived neurons at 12 and 30 WPD. Insets show RFP expression of recorded neurons.

(B) An hPSC-derived neuron labeled by intracellular filling with neurobiotin immunostained positive for SST at 30 WPD.

(C) Representative AP firing patterns at each stage upon near threshold (top) and superthreshold (bottom) current injection, and AP velocity (dV/dt) at threshold firing (middle). Scale bar represent 50 mV or 40 Vs^{-1} for dV/dt, 100 ms.

See also Figure S6.

(D) Average first AP traces upon threshold current injection. Scale bars represent 25 mV and 25 ms (the dashed line represents the baseline).

(E) Statistical results showing AHPs at each stage.

(F–G) I–V curve of Na^+ (F) and K^+ currents (G) at each stage, measured under stepped voltages (500 ms duration).

(H) Representative AP firing patterns of 22 gestational week (gw) human fetal cortical neurons upon near threshold (upper) and superthreshold (lower) current injection. Scale bars represent 50 mV and 100 ms.

(I) Statistical results showing membrane resistance (Rm), resting membrane potential (RMP), membrane capacitance (Cm), and action potential (AP) half-width.

(E, F, G, and I) Data are represented as mean ± SEM. **, $p < 0.01$; ***, $p < 0.001$.

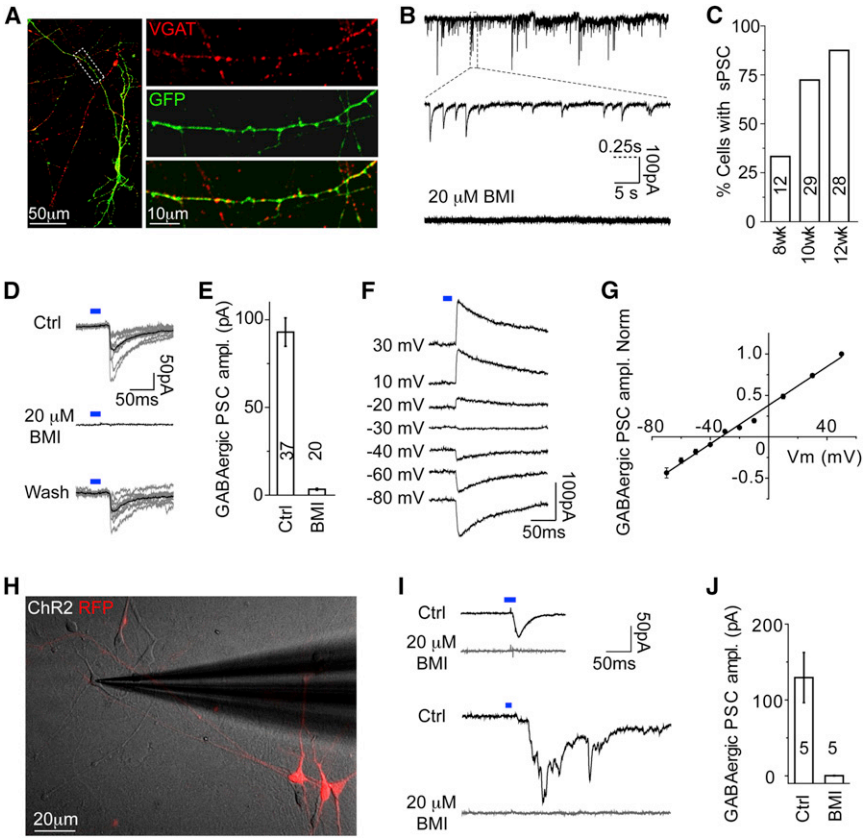

Figure 6. Functional GABAergic Synaptic Properties of hPSC-Derived Interneurons

(A) Images showing VGAT expression in hPSC-derived *NKX2.1*-GFP+ neurons at 12 WPD. Right, zoom of dashed rectangle. The scale bar represents 50 μm (left) and 10 μm (right).

(B) Traces showing spontaneous postsynaptic currents (PSCs) in hPSC-derived neurons. Bottom, PSCs were fully blocked by BMI. The scale bar represents 100 pA and 5 s and 0.25 s (dashed line) for the middle trace.

(C) Percentage of neurons showing spontaneous PSCs at different stages.

(D) hPSC-derived neurons were transfected with ChR2-EYFP. Traces show pulses of blue light (blue bar)-evoked PSCs in neighboring cells that were reversibly blocked by BMI. The scale bar represents 50 pA and 50 ms.

See also Figure S6.

(E) Average amplitudes of light-evoked GABAergic PSCs and application of BMI.

(F and G) Traces showing light-evoked (blue bar) PSCs at different holding potentials. Summarized results (n = 7) showing the I–V curve of light-evoked GABAergic PSCs (G).

(H) A merged image showing DIC of human fetal cortical cells cocultured with sorted *UbC*-RFP+ and ChR2-transfected hPSC-derived neurons. The scale bar represents 20 μm.

(I) Traces showing blue light (blue bar) stimulation of hPSC-derived neuron-evoked PSCs in RFP-negative recorded human fetal cortical neurons. Upper panel shows PSC mono-synaptic response. The lower panel shows PSC with polysynaptic responses—both fully blocked by BMI. The scale bar represents 50pA and 50 ms.

(J) Averaged amplitudes of light-evoked PSCs and application of BMI.

(E and J) Data are represented as mean ± SEM.

channelrhodopsin2-EYFP (ChR2-EYFP). Blue light stimulation reliably induced AP firing in EYFP+ neurons (Figure S6F) and evoked robust postsynaptic currents (PSCs) in neighboring neurons (Figures 6D and 6E). In addition, the PSCs showed a long decay time (31.4 ± 1.9 ms, n = 26), which was characteristic of GABAergic PSCs. This was further verified by the reversible blockade of light-evoked PSCs by BMI (Figures 6D and 6E). The reversal potential of light-evoked PSCs was −32.7 mV (Figures 6F and 6G), close to the expected Cl^- reversal potential under our recording conditions (−37.3 mV = −53.4 mV [by Nernst equation] + 16.1 mV [junction potential]). These results demonstrated that the hPSC-derived neurons produced exclusively GABAergic synaptic output.

To examine whether hPSC-derived interneurons could form synapses onto primary human neurons, we labeled MGE-like cells at 4 WPD with ChR2-YFP and *UbC*-RFP virus, and RFP+ FACS-sorted cells were cocultured for 7 weeks with dissociated human fetal cortical cells from 20 gw. Whole-cell recordings were obtained from RFP− primary cortical neurons after coculture (Figure 6H). Blue light stimulation of hPSC-derived neurons induced GABAergic-specific PSCs in recorded primary neurons that were completely blocked by BMI (Figures 6I and 6J). Furthermore, upon light stimulation, we found polysynaptic responses (Figure 6I), which were also blocked by BMI, indicating robust GABAergic synaptic integration of hPSC-derived neurons into cultured human fetal neuronal circuits.

hPSC-Derived Interneuron Subtype Maturation and Functional Integration in the Mouse Brain

To rigorously evaluate cell fate and function, we transplanted hPSC-derived MGE-like cells into the mouse brain. We modified our protocol to avoid the injection of undifferentiated NKX2.1+ neural stem cells and to increase interneuron subtype maturation (see Supplemental Experimental Procedures and Table S2). Fluorescence-activated cell sorting (FACS) purification was used to select for neuronal precursors expressing PSA-NCAM (Schmandt et al., 2005). An average of 75.7% ± 5.2% (n = 12) of *NKX2.1*-GFP+ cells were positive for PSA-NCAM expression (Figure S7A). *NKX2.1*-GFP+ and PSA-NCAM+ cells from day 35 ML or day 50 aEB cultures were sorted, some cells were labeled with *UbC*-RFP or *Synapsin*-YFP virus, and were injected into severe combined immunodeficient (SCID) newborn mouse cortices (Figure 7A).

Human cells, detected by staining for human-specific nuclear antigen (HNA), survived for up to 7 months postinjection (MPI) (the longest time point) and did not form tumors. Human cell-survival rates (percentage of injected cells) after 2, 4, and 7 MPI were 5.6% ± 2.6%, 3.1% ± 1.5%, and 8.6% ± 3.1%,

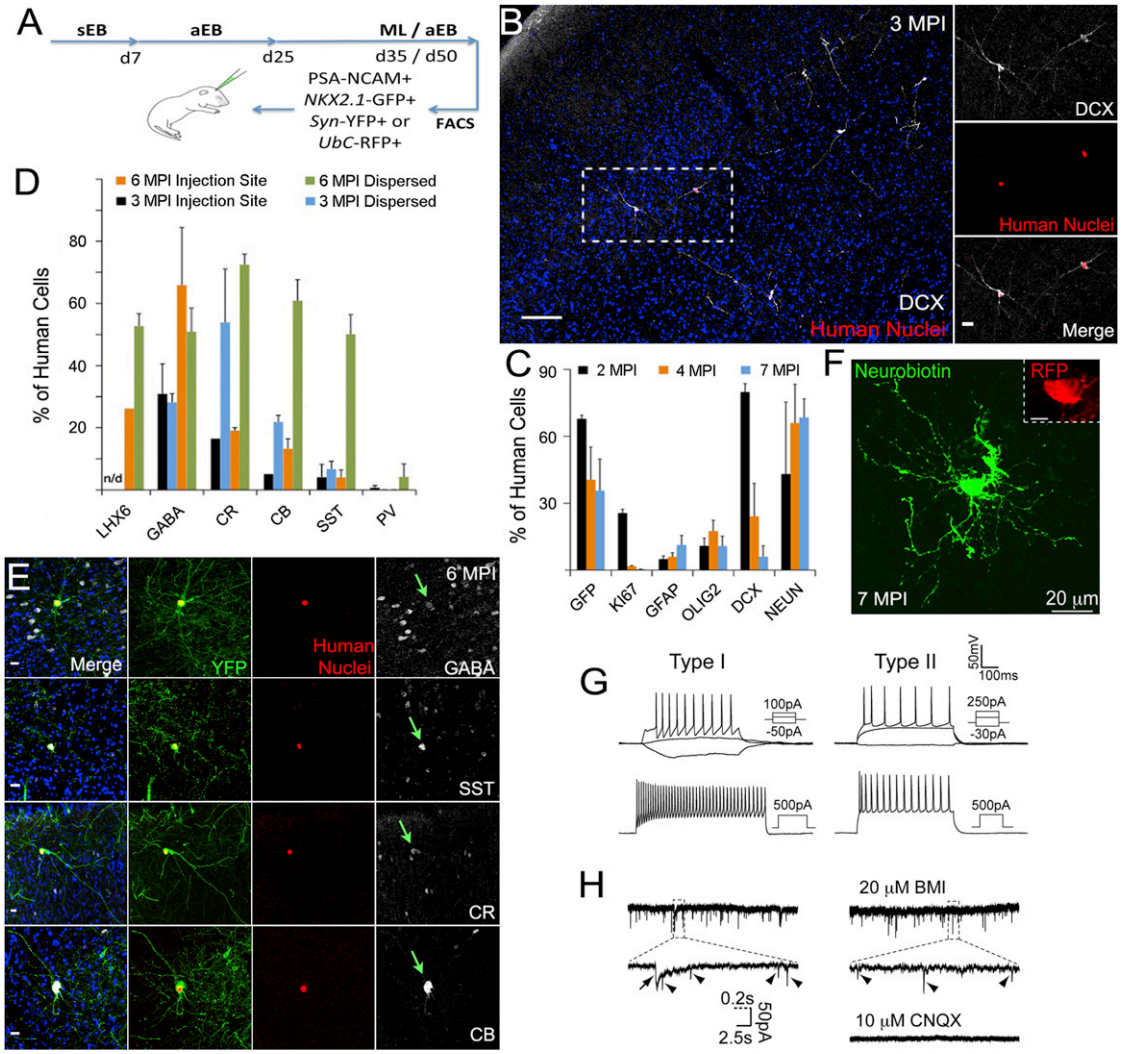

Figure 7. hPSC-Derived Interneuron Subtype Maturation and Functional Integration in the Mouse Brain

(A) hPSC-derived MGE-like interneuron precursors FACS-sorted for *NKX2.1*-GFP and PSA-NCAM, labeled with YFP or RFP virus, and injected into newborn mouse cortex.

See also Supplemental Experimental Procedures and Table S2.

(B) Human nuclei+ cells expressed DCX and migrated into the cortex by 3 months postinjection (MPI). DAPI expression is shown in blue. The scale bar represents 100 μm. Right, a zoom of dashed rectangle in separate channels and merged. The scale bar represents 20 μm.

See also Figure S7.

(C and D) A quantification of lineage-specific marker histology at 2 (black), 4 (orange), and 7 (blue) MPI with d35 ML cells (C) or subtype markers at 3 (black, blue) and 6 (orange, green) MPI with d50 aEB cells (D) plotted as human cells near or dispersed from the injection site. Data are represented as mean ± SEM.

(E) A histological analysis of human nuclei+ cells prelabeled with *Syn*-YFP at 6 MPI that coexpressed (arrow) subtype markers. DAPI expression is shown in blue. The scale bar represents 20 μm.

See also Figure S5.

(F) An hPSC-derived neuron labeled by intracellular filling of neurobiotin (NB, green). The inset shows *UbC*-RFP fluorescence of a filled neuron at 7 MPI. The scale bar represents 20 μm, the inset scale bar represents 5 μm.

(G) Traces of AP firing patterns of type I (left) and type II (right) hPSC-derived neurons upon near-threshold (top) and superthreshold (bottom) current injection at 7 MPI. Scale bars represent 50 mV and 100 ms.

See also Figure S7.

(H) Left, traces of spontaneous PSCs recorded from hPSC-derived neurons at 7 MPI. Upper right, BMI-blocked PSCs with slow decay time (arrow) and the remaining PSCs with fast decay time (arrow head) were blocked by the subsequent application of CNQX (lower right panel). Scale bars represent 50 pA and 2.5 s and 0.2 s (dashed line) for zoomed traces.

respectively. By 2 MPI, human cells expressing HNA and *NKX2.1*-GFP (67.8% ± 1.6%), KI67 (25.5% ± 1.7%), or DCX (79.8% ± 3.8%) were mostly still located near the injection site (Figure S7B). But, by 3 to 7 MPI, a fraction of the human cells migrated more than 1 mm rostral and caudal into the mouse cortex (Figures 7B and S7C). KI67 and DCX expression were

significantly reduced over time (1.7% ± 0.27%, p = 0.04; 5.9% ± 4.9%, p = 0.008), and *NKX2.1*-GFP was similarly downregulated (35.6% ± 14% by 7 MPI). The opposite trend was found for the postmitotic neuronal marker (NEUN) which increased to 68.4% ± 8.3% of human cells by 7 MPI (Figure 7C), suggesting the maturation of NKX2.1− and NKX2.1+ cortical- and striatal-like interneurons.

To quantify subtype maturation, we separated dispersed human cells from those that remained at the injection site. Interestingly, dispersed cells exhibited increased subtype marker expression that also correlated with time postinjection (Figures 7D and 7E), especially for SST. Similar to in vitro maturation, dispersed human cells expressed LHX6 (52.7% ± 4%), GABA (50.9% ± 7%), CB (60.9% ± 7%), CR (72.5% ± 3%), and SST (50.1% ± 6%) by 6 MPI, and rare PV+ cells were detected. Human cells remaining at the injection site did not robustly express subtype markers, but they appeared to be GABAergic neurons expressing GABA (65.9% ± 18%) and NEUN (77.7% ± 4%). In summary, hPSC-derived MGE-like neuronal precursors injected into the mouse brain gradually matured into GABAergic interneuron subtypes.

Lastly, to examine whether hPSC-derived MGE-like cells could develop into functional interneurons that synaptically integrate in vivo, we performed whole-cell recordings of RFP+ human cells in mouse brain slices at 7 MPI. Intracellular filling with neurobiotin and poststaining revealed the extensive process branching of recorded RFP+ neurons (Figure 7F). Among 17 total human cells patched from three animals, 16 neurons exhibited the ability to fire APs with an average RMP of −64.8 ± 4.0 mV. In addition, two groups of interneurons were identified (type I and type II) with different membrane properties and firing patterns. Type I interneurons had an average RMP of −67.3 ± 2.9 mV, Rm of 257 ± 78 MΩ, and Cm of 69.4 ± 0.6 pF (n = 4). The firing pattern of type I interneurons displayed a significant delay to spike at threshold and little adaptation upon superthreshold current injection (Figures 7G and S7D). Type II interneurons had more hyperpolarized RMP (−80.1 ± 3.4 mV), smaller Rm (91 ± 28 MΩ), and smaller Cm (27.7 ± 4.6 pF) (n = 4). The firing pattern of type II interneurons showed rapid adaptation of initial spikes upon superthreshold current injection (Figures 7G and S7E). Furthermore, the transplanted hPSC-derived interneurons received synaptic inputs (16 of 16) containing both BMI-sensitive GABAergic and 6-Cyano-2, 3-dihydroxy-7-nitro-quinoxaline (CNQX)-sensitive glutamatergic components (Figure 7H), suggesting functional integration into the host cortex.

DISCUSSION

Here, we model functional human telencephalic-like interneuron subtype maturation from hPSCs and demonstrate their protracted acquisition of mature features. First, we show that hPSC-derived MGE-like progenitors develop through an additional type of radial glial-like stem cell enriched in the human brain. Second, we chronicle the functional maturation of hPSC-derived MGE-like precursors into subtypes of interneurons that slowly develop advanced physiological properties over a prolonged period of time. Third, we find their maturation in vitro and posttransplantation parallels the temporal developmental sequence of endogenous human interneurons.

First, MGE-like cells were derived from hPSCs with a robust B27+5F method that harnessed signaling pathways involved in embryonic forebrain development (Rallu et al., 2002; Watanabe et al., 2007). Previously, HES-3 *NKX2.1*$^{GFP/w}$ hESCs were differentiated into hypothalamic forebrain-like precursors in the presence of FGF2 and retinoic acid (RA) (Goulburn et al., 2011). In contrast to this protocol, we detected earlier FOXG1 expression, along with downregulation of NKX2.2 protein, and we did not find RAX expression. Therefore, the B27+5F method favors telencephalic MGE-like differentiation, whereas the FGF2-RA method may be useful for diencephalic hypothalamus-like derivation.

An additional type of radial glial stem cell is enriched in the developing human cortical OSVZ, which may contribute to the expanded size of the human brain (Lui et al., 2011). We have also observed these oRG-like cells in the human fetal MGE (data not shown). Here, we used live-cell imaging to observe oRG-like, as well as vRG-like, mitotic behaviors in our hPSC-derived MGE-like cultures. In addition to the expansion of neuron numbers, the oRG stem cell stage likely contributes to the extended developmental timeline of human cortical interneurons and pyramidal neurons by delaying their birth. Additional study is needed to determine if oRGs are required for the maturation of certain neuronal subtypes.

Second, hPSC-derived MGE-like progenitors matured into mixed cortical- and striatal-like GABAergic interneuron lineages that expressed SST, CR, and CB subtype markers over a 30 week timeline. In association with protracted morphological and subtype marker maturation, the functional electrophysiological properties of hPSC-derived interneurons also exhibited slow maturation over 30 WPD. Previous work showed that the development of hPSC-derived neuronal firing properties correlated with increasing voltage-gated Na^+ and K^+ currents between 4 and 7 WPD (Johnson et al., 2007). Similarly, we found that the amplitude of voltage-gated Na^+ and K^+ currents in our hPSC-derived interneurons increased from 8 to 12 WPD. However, mature hPSC-derived interneuron subtype firing properties were not observed until 30 WPD, despite no further increase in average Na^+ and K^+ currents after 12 WPD, suggesting that more mature firing properties may result from subtype-specific channel expression (Goldberg et al., 2011). We did not detect the fast-spiking PV+ interneuron subtype by 30 WPD. Given that primary PV+ cells are not detected in the cortex until postnatal stages, additional time may be required for their maturation from hPSCs. We observed immature cells that express PV by 15 WPD; however, this lineage disappeared at later stages, suggesting that conditions may need to be optimized for their maturation as well. Additional methods will also need to be developed in order to preferentially direct the differentiation of either cortical or striatal interneuron lineages or to purify a particular lineage.

After injection into the mouse brain, hPSC-derived interneuron precursors survived, dispersed from the injection site, matured into subtypes, and functionally integrated into the host cortex. The human cell-survival rate was 3%–8% of injected cells and is most likely an underestimate because of the efflux of human cells out of the needle tract at the time of injection. Nevertheless, this rate is not far off from primary mouse fetal MGE cell-transplant survival rates of ~10%–20%. It is also similar to the 2%–10% of mouse ESC-derived MGE-like cells that survived postinjection into the mouse cortex (Maroof et al., 2010). Furthermore,

prior reports demonstrated that 1%–3% survival of injected primary mouse MGE cells was sufficient for behavioral improvements in rodent models of Parkinson's disease and neuropathic pain (Bráz et al., 2012; Martínez-Cerdeño et al., 2010). Thus, the hPSC-derived MGE-like cell-survival rate may be sufficient for future cell-therapy-based applications.

The human MGE-like cells migrated 1–2 mm into the rodent cortex postinjection, similar to mouse ESC-derived MGE-like cells (Maroof et al., 2010). But, they did not migrate as extensively as primary mouse fetal MGE cells, and some cells remained at the injection site. This suggests that optimization of the PSC differentiation stage and/or the development of methods to purify migratory MGE-like cells may be needed. Interestingly, the increased expression of interneuron subtype markers correlated with the dispersed fraction of hPSC-derived cells. The interneuron subtypes and protracted timing of marker upregulation postinjection were similar to in vitro hPSC maturation. By 7 MPI, we identified two groups (type I and II) of hPSC-derived interneurons displaying distinct firing properties. Type I neurons resembled adult mouse delayed-spiking (DS) interneurons or nonrebounding regular-spiking nonpyramidal cells (NR-RSNPs), which were found to express SST (Butt et al., 2005), and type II neurons were comparable to adult mouse non-fast-spiking (NFS1 or NFS2) interneurons that were found to express SST or CR (Miyoshi et al., 2007; Sousa et al., 2009)—which was consistent with hPSC-derived interneuron subtypes. However, the subtype marker expression profiles of type I and II hPSC-derived interneurons remain to be determined.

Despite the slow maturation of interneuron subtype firing properties, we detected GABAergic synaptic activity of hPSC-derived interneurons beginning 8 WPD. We used optogenetics to demonstrate robust synaptic integration of hPSC-derived interneurons into cultured primary human neuronal networks. We also detected both GABAergic and glutamatergic synaptic inputs into hPSC-derived interneurons 7 MPI into the mouse cortex. Because the hPSC-derived neurons produced GABAergic-exclusive output, glutamatergic synaptic inputs were most likely from host mouse excitatory neurons, indicating that hPSC-interneurons are capable of integrating into host cortical circuits.

Third, the protracted maturation of hPSC-derived interneuron subtype marker expression and firing properties paralleled endogenous human interneuron development. Similar interneuron subtypes were found in the human fetal and infant cortex, and in cultures derived from the human fetal MGE. Moreover, the sequence and timing of subtype marker expression was conserved. These resemblances, and the observation that hPSC-derived interneuron maturation is not accelerated by coculture or transplantation, suggest that interneuron maturation is an intrinsic program analogous to other MGE interneuron intrinsic programs of plasticity induction and cell death (Southwell et al., 2010; Southwell et al., 2012). In an attempt to estimate neuronal age, we recorded neurons from 22 gw human fetal cortical plate neurons and found their AP firing and membrane properties to be considerably immature (Figure 5H and 5I), in agreement with a previous study (Moore et al., 2009), in comparison to the 30 WPD hPSC-derived interneurons. The hPSC-derived interneurons may represent an early postnatal stage, an observation that is based on similarities to the physiological properties of early-adult nonhuman primate interneurons (Zaitsev et al., 2009).

In conclusion, we report the stepwise functional maturation of human interneuron subtypes through an hPSC-derived MGE-like intermediate, and we demonstrate the protracted intrinsic development of mature features that model aspects of endogenous postnatal interneurons. The maturation of patient iPSC-derived functional cell types to a postnatal, or more advanced, stage may be critical for creating meaningful disease models, as well as for drug efficacy or toxicity screens. Consistent with this notion, it was reported that hPSC-derived cardiomyocytes only recapitulated adult-onset heart disease phenotypes when adult-stage features had been achieved (Kim et al., 2013). Accordingly, hPSC-derived SST+ interneuron subtypes, which required 20–30 WPD for functional maturation, may be affected in adult temporal lobe epilepsy (de Lanerolle et al., 2003; Robbins et al., 1991) and may provide a substrate to identify drugs that enhance their function. Our findings also provide a framework for future patient iPSC modeling of diseases linked to interneuron dysfunction. However, given that many diseases are adult onset, hPSC-derived interneurons may need to be matured even more to be useful. On the basis of their remarkably lengthy timeline, it will be interesting to study the mechanisms regulating human interneuron maturation and to possibly uncover a means to accelerate their development. Discoveries along these lines would facilitate hPSC-based regenerative medicine applications.

EXPERIMENTAL PROCEDURES

Cell Culture

HES-3 hESCs were maintained on irradiated mouse embryonic fibroblasts (Millipore) in knockout Dulbecco's modified Eagle's medium with 20% knockout serum replacement, 1% nonessential amino acids (NEAA), 1% pen-strep-glutamine, 0.0008% 2-mercaptoethanol, and 10 ng/mL FGF-basic (Invitrogen). Differentiation was initiated by collagenase IV and dispase (1 mg/mL each; Invitrogen) preferential selection for hESC colonies. Colonies were trypsinized to single cells, and, as described (Eiraku et al., 2008), ~10,000 cells/well were plated into low-attachment, round-bottom 96-well plates (Corning or the NOF Group) to form 1 sEB/well in optimized B27+5F differentiation medium 1, which consisted of Neurobasal-A, 2% B27-vitamin A (Invitrogen), and the same supplements in hESC media with the exception of FGF-basic. Also, Y27632 (10 μM), SB431542 (10 μM), purmorphamine (1–2 μM) (Stemgent), BMPRIA-Fc (1.5 μg/mL), and DKK1 (1 μg/mL) (Invitrogen) were added. See Supplemental Experimental Procedures for more information. All experiments conducted on hESCs and human fetal tissue adhered to approved University of California, San Francisco (UCSF), Stem Cell Research Oversight Committee and Committee on Human Research protocols.

Transplantation

Excess medium was removed from sorted cell pellets for the creation of concentrated cell suspensions of 1,000 cells/nl. Cells were loaded into a beveled glass micropipette (Wiretrol 5 ul, Drummond Scientific Company) mounted on a stereotactic hydraulic injector. P2 CB.17-SCID pups (Charles River Laboratories) were anesthetized through hypothermia and positioned in a clay head mold on the injector platform. For each pup, 10–100,000 cells per injection site were delivered transcranially into the right cerebral cortex 0.9 mm from the midline (sagittal sinus) and 2.6 mm from the lambda. The depth of injection was 0.45 mm from the skin surface. All transplantation experiments adhered to approved UCSF Institutional Animal Care and Use Committee protocols.

Immunostaining

Cultured cells were fixed in 4% paraformaldehyde for 10–20 min. Mouse brains were fixed overnight at 4°C after transcardial perfusion and sectioned

(50 μm) by vibratome or sliding microtome. EBs and human tissue were sectioned (25 μm) by cryostat. Cells and sections were stained by 5–10 min antigen retrieval with boiling 0.01 M citrate buffer (pH = 6), 1 hr block with 5% serum and 0.1% Triton X-100 in PBS, overnight 4°C primary antibody in block buffer (except triton-free buffer was used for the GABA antibody), washing three times in PBS+Triton X-100, treatment with 2 hr secondary antibody (Invitrogen), and washing four times in PBS+Triton X-100. Primary antibodies are listed in Table S3.

Transcript Expression

RNA was prepared from cell pellets with the RNeasy Kit (QIAGEN). Complementary DNA was prepared with a Superscript III First-Strand Kit (Invitrogen). qRT-PCR was performed with SYBR Green Master Mix on a real-time PCR system (Applied Biosystems). RT negative controls were used. Amplicon specificity was determined by gel electrophoresis and melt-curve analysis. Primer sequences are listed in Table S3.

For microarray analysis, RNA was submitted to the Southern California Genotyping Consortium for hybridization to Illumina HumanHT-12 v4.0 Expression BeadChip. hESCs contained one sample and four technical replicates, D20 contained three independent samples, D35 contained one sample and two technical replicates, and D55 contained one sample and one technical replicate. Data were analyzed with GenomeStudio (Illumina) software. Probes without signal were validated by confirming hybridization to control human brain reference RNA and/or to samples archived in ArrayExpress.

Electrophysiology and Optical Methods

The patch electrodes were made from borosilicate glass capillaries (B-120-69-15, Sutter Instruments) with a resistance in the range of 5–7 MΩ. The pipettes were tip-filled with internal solution containing 125 mM K-gluconate, 15 mM KCl, 10 mM HEPES, 4 mM MgCl2, 4 mM Na2ATP, 0.3 mM Na3GTP, 10 mM Tris-phosphocreatine, and 0.2 mM EGTA. See Supplemental Experimental Procedures for more information.

Statistical Analyses

Data are presented as mean ± SEM. In Figure 2E, data are represented as the mean percentage of coexpressing cells. In Figures 3C–3H, data are shown as mean bead signal intensity. In Figure 4C, data are shown as a mean percentage of UbC-RFP+, ChR2-YFP+, or TUJ+ neurons. In Figures 7C–7D, data are shown as a mean percentage of HNA^+ or UbC-RFP+ human cells. Statistical comparisons used one-way ANOVA with a post hoc Bonferroni test for electrophysiology data and used a two-tailed, two-sample unequal variance Student's t test for immunostaining data. Cell counts were calculated with Imaris (Bitplane) software with the MATLAB plugin. A summary of sample sizes and cell counts for each experiment and marker is listed in Table S4.

ACCESSION NUMBERS

Microarray data were deposited in the Gene Expression Omnibus (GEO) and can be found at accession number GSE45660.

SUPPLEMENTAL INFORMATION

Supplemental Information contains Supplemental Experimental Procedures, seven figures, four tables, and three movies and can be found with this article online at http://dx.doi.org/10.1016/j.stem.2013.04.005.

ACKNOWLEDGMENTS

We thank S. Baraban, R. Hunt, D. Wang, S. Gee, P. Parker, and M. Yang for electrophysiology guidance and discussion. We thank D. Hansen, J. Lui, M. Oldham, M. Paredes, C. Harwell, X. Wang, S. Wang, Y. Wang, S. Hart, R. Romero, T. Nguyen, and W. Walantus for helpful discussion, gene expression, cell culture, tissue procurement, processing, and technical assistance. We thank K. Probst for graphical design. We thank M. Ramalho-Santos and Y. Ohi for hiPSC lines, K. Deisseroth for the ChR2-EYFP plasmid, and K. Yoshikawa for the DLX2 antibody. We thank the staff and faculty at the San Francisco General Hospital Women's Options Center and at Advanced Bioscience Resources who assisted in human fetal tissue collection. This work was supported by the California Institute of Regenerative Medicine (RC1-00346 to A.R.K., RB2-01602 to J.L.R.R., and TR2-01749 to A.A.-B.), the National Institute of Neurological Disorders and Stroke, and the Osher Foundation. J.C. is a recipient of the CARE & CURE Pediatric Epilepsy Fellowship from Epilepsy Foundation of Greater Los Angeles. A.G.E. and E.G.S. are Senior Research Fellows of the National Health and Medical Research Council of Australia. C.R.N., A.A.-B., J.L.R.R., and A.R.K. are cofounders, board members, and shareholders of Neurona Therapeutics.

Received: September 21, 2012
Revised: February 22, 2013
Accepted: April 8, 2013
Published: May 2, 2013

REFERENCES

Anderson, S.A., Marín, O., Horn, C., Jennings, K., and Rubenstein, J.L. (2001). Distinct cortical migrations from the medial and lateral ganglionic eminences. Development *128*, 353–363.

Bráz, J.M., Sharif-Naeini, R., Vogt, D., Kriegstein, A., Alvarez-Buylla, A., Rubenstein, J.L., and Basbaum, A.I. (2012). Forebrain GABAergic neuron precursors integrate into adult spinal cord and reduce injury-induced neuropathic pain. Neuron *74*, 663–675.

Butt, S.J., Fuccillo, M., Nery, S., Noctor, S., Kriegstein, A., Corbin, J.G., and Fishell, G. (2005). The temporal and spatial origins of cortical interneurons predict their physiological subtype. Neuron *48*, 591–604.

Chambers, S.M., Fasano, C.A., Papapetrou, E.P., Tomishima, M., Sadelain, M., and Studer, L. (2009). Highly efficient neural conversion of human ES and iPS cells by dual inhibition of SMAD signaling. Nat. Biotechnol. *27*, 275–280.

Chao, H.T., Chen, H., Samaco, R.C., Xue, M., Chahrour, M., Yoo, J., Neul, J.L., Gong, S., Lu, H.C., Heintz, N., et al. (2010). Dysfunction in GABA signalling mediates autism-like stereotypies and Rett syndrome phenotypes. Nature *468*, 263–269.

Cheah, C.S., Yu, F.H., Westenbroek, R.E., Kalume, F.K., Oakley, J.C., Potter, G.B., Rubenstein, J.L., and Catterall, W.A. (2012). Specific deletion of NaV1.1 sodium channels in inhibitory interneurons causes seizures and premature death in a mouse model of Dravet syndrome. Proc. Natl. Acad. Sci. USA *109*, 14646–14651.

Cobos, I., Calcagnotto, M.E., Vilaythong, A.J., Thwin, M.T., Noebels, J.L., Baraban, S.C., and Rubenstein, J.L. (2005). Mice lacking Dlx1 show subtype-specific loss of interneurons, reduced inhibition and epilepsy. Nat. Neurosci. *8*, 1059–1068.

de Lanerolle, N.C., Kim, J.H., Williamson, A., Spencer, S.S., Zaveri, H.P., Eid, T., and Spencer, D.D. (2003). A retrospective analysis of hippocampal pathology in human temporal lobe epilepsy: evidence for distinctive patient subcategories. Epilepsia *44*, 677–687.

Eiraku, M., Watanabe, K., Matsuo-Takasaki, M., Kawada, M., Yonemura, S., Matsumura, M., Wataya, T., Nishiyama, A., Muguruma, K., and Sasai, Y. (2008). Self-organized formation of polarized cortical tissues from ESCs and its active manipulation by extrinsic signals. Cell Stem Cell *3*, 519–532.

Elkabetz, Y., Panagiotakos, G., Al Shamy, G., Socci, N.D., Tabar, V., and Studer, L. (2008). Human ES cell-derived neural rosettes reveal a functionally distinct early neural stem cell stage. Genes Dev. *22*, 152–165.

Espuny-Camacho, I., Michelsen, K.A., Gall, D., Linaro, D., Hasche, A., Bonnefont, J., Bali, C., Orduz, D., Bilheu, A., Herpoel, A., et al. (2013). Pyramidal neurons derived from human pluripotent stem cells integrate efficiently into mouse brain circuits in vivo. Neuron *77*, 440–456.

Fazzari, P., Paternain, A.V., Valiente, M., Pla, R., Luján, R., Lloyd, K., Lerma, J., Marín, O., and Rico, B. (2010). Control of cortical GABA circuitry development by Nrg1 and ErbB4 signalling. Nature *464*, 1376–1380.

Fertuzinhos, S., Krsnik, Z., Kawasawa, Y.I., Rasin, M.R., Kwan, K.Y., Chen, J.G., Judas, M., Hayashi, M., and Sestan, N. (2009). Selective depletion of

molecularly defined cortical interneurons in human holoprosencephaly with severe striatal hypoplasia. Cereb. Cortex *19*, 2196–2207.

Fietz, S.A., Kelava, I., Vogt, J., Wilsch-Bräuninger, M., Stenzel, D., Fish, J.L., Corbeil, D., Riehn, A., Distler, W., Nitsch, R., and Huttner, W.B. (2010). OSVZ progenitors of human and ferret neocortex are epithelial-like and expand by integrin signaling. Nat. Neurosci. *13*, 690–699.

Goldberg, E.M., Jeong, H.Y., Kruglikov, I., Tremblay, R., Lazarenko, R.M., and Rudy, B. (2011). Rapid developmental maturation of neocortical FS cell intrinsic excitability. Cereb. Cortex *21*, 666–682.

Goulburn, A.L., Alden, D., Davis, R.P., Micallef, S.J., Ng, E.S., Yu, Q.C., Lim, S.M., Soh, C.L., Elliott, D.A., Hatzistavrou, T., et al. (2011). A targeted NKX2.1 human embryonic stem cell reporter line enables identification of human basal forebrain derivatives. Stem Cells *29*, 462–473.

Hansen, D.V., Lui, J.H., Parker, P.R., and Kriegstein, A.R. (2010). Neurogenic radial glia in the outer subventricular zone of human neocortex. Nature *464*, 554–561.

Johnson, M.A., Weick, J.P., Pearce, R.A., and Zhang, S.C. (2007). Functional neural development from human embryonic stem cells: accelerated synaptic activity via astrocyte coculture. J. Neurosci. *27*, 3069–3077.

Kim, J.E., O'Sullivan, M.L., Sanchez, C.A., Hwang, M., Israel, M.A., Brennand, K., Deerinck, T.J., Goldstein, L.S., Gage, F.H., Ellisman, M.H., and Ghosh, A. (2011). Investigating synapse formation and function using human pluripotent stem cell-derived neurons. Proc. Natl. Acad. Sci. USA *108*, 3005–3010.

Kim, C., Wong, J., Wen, J., Wang, S., Wang, C., Spiering, S., Kan, N.G., Forcales, S., Puri, P.L., Leone, T.C., et al. (2013). Studying arrhythmogenic right ventricular dysplasia with patient-specific iPSCs. Nature *494*, 105–110.

Kriegstein, A.R., and Götz, M. (2003). Radial glia diversity: a matter of cell fate. Glia *43*, 37–43.

Le Magueresse, C., and Monyer, H. (2013). GABAergic interneurons shape the functional maturation of the cortex. Neuron *77*, 388–405.

Li, X.J., Zhang, X., Johnson, M.A., Wang, Z.B., Lavaute, T., and Zhang, S.C. (2009). Coordination of sonic hedgehog and Wnt signaling determines ventral and dorsal telencephalic neuron types from human embryonic stem cells. Development *136*, 4055–4063.

Lui, J.H., Hansen, D.V., and Kriegstein, A.R. (2011). Development and evolution of the human neocortex. Cell *146*, 18–36.

Ma, L., Hu, B., Liu, Y., Vermilyea, S.C., Liu, H., Gao, L., Sun, Y., Zhang, X., and Zhang, S.C. (2012). Human embryonic stem cell-derived GABA neurons correct locomotion deficits in quinolinic acid-lesioned mice. Cell Stem Cell *10*, 455–464.

Markram, H., Toledo-Rodriguez, M., Wang, Y., Gupta, A., Silberberg, G., and Wu, C. (2004). Interneurons of the neocortical inhibitory system. Nat. Rev. Neurosci. *5*, 793–807.

Maroof, A.M., Brown, K., Shi, S.H., Studer, L., and Anderson, S.A. (2010). Prospective isolation of cortical interneuron precursors from mouse embryonic stem cells. J. Neurosci. *30*, 4667–4675.

Martínez-Cerdeño, V., Noctor, S.C., Espinosa, A., Ariza, J., Parker, P., Orasji, S., Daadi, M.M., Bankiewicz, K., Alvarez-Buylla, A., and Kriegstein, A.R. (2010). Embryonic MGE precursor cells grafted into adult rat striatum integrate and ameliorate motor symptoms in 6-OHDA-lesioned rats. Cell Stem Cell *6*, 238–250.

Miyoshi, G., Butt, S.J., Takebayashi, H., and Fishell, G. (2007). Physiologically distinct temporal cohorts of cortical interneurons arise from telencephalic Olig2-expressing precursors. J. Neurosci. *27*, 7786–7798.

Moore, A.R., Filipovic, R., Mo, Z., Rasband, M.N., Zecevic, N., and Antic, S.D. (2009). Electrical excitability of early neurons in the human cerebral cortex during the second trimester of gestation. Cereb. Cortex *19*, 1795–1805.

Nóbrega-Pereira, S., Gelman, D., Bartolini, G., Pla, R., Pierani, A., and Marín, O. (2010). Origin and molecular specification of globus pallidus neurons. J. Neurosci. *30*, 2824–2834.

Rallu, M., Corbin, J.G., and Fishell, G. (2002). Parsing the prosencephalon. Nat. Rev. Neurosci. *3*, 943–951.

Robbins, R.J., Brines, M.L., Kim, J.H., Adrian, T., de Lanerolle, N., Welsh, S., and Spencer, D.D. (1991). A selective loss of somatostatin in the hippocampus of patients with temporal lobe epilepsy. Ann. Neurol. *29*, 325–332.

Schmandt, T., Meents, E., Gossrau, G., Gornik, V., Okabe, S., and Brüstle, O. (2005). High-purity lineage selection of embryonic stem cell-derived neurons. Stem Cells Dev. *14*, 55–64.

Shi, Y., Kirwan, P., Smith, J., Robinson, H.P., and Livesey, F.J. (2012). Human cerebral cortex development from pluripotent stem cells to functional excitatory synapses. Nat. Neurosci. *15*, 477–486, S1.

Shimamura, K., and Rubenstein, J.L. (1997). Inductive interactions direct early regionalization of the mouse forebrain. Development *124*, 2709–2718.

Sousa, V.H., Miyoshi, G., Hjerling-Leffler, J., Karayannis, T., and Fishell, G. (2009). Characterization of Nkx6-2-derived neocortical interneuron lineages. Cereb. Cortex *19*(*Suppl 1*), i1–i10.

Southwell, D.G., Froemke, R.C., Alvarez-Buylla, A., Stryker, M.P., and Gandhi, S.P. (2010). Cortical plasticity induced by inhibitory neuron transplantation. Science *327*, 1145–1148.

Southwell, D.G., Paredes, M.F., Galvao, R.P., Jones, D.L., Froemke, R.C., Sebe, J.Y., Alfaro-Cervello, C., Tang, Y., Garcia-Verdugo, J.M., Rubenstein, J.L., et al. (2012). Intrinsically determined cell death of developing cortical interneurons. Nature *491*, 109–113.

Verret, L., Mann, E.O., Hang, G.B., Barth, A.M., Cobos, I., Ho, K., Devidze, N., Masliah, E., Kreitzer, A.C., Mody, I., et al. (2012). Inhibitory interneuron deficit links altered network activity and cognitive dysfunction in Alzheimer model. Cell *149*, 708–721.

Wang, Y., Li, G., Stanco, A., Long, J.E., Crawford, D., Potter, G.B., Pleasure, S.J., Behrens, T., and Rubenstein, J.L. (2011). CXCR4 and CXCR7 have distinct functions in regulating interneuron migration. Neuron *69*, 61–76.

Watanabe, K., Ueno, M., Kamiya, D., Nishiyama, A., Matsumura, M., Wataya, T., Takahashi, J.B., Nishikawa, S., Nishikawa, S., Muguruma, K., and Sasai, Y. (2007). A ROCK inhibitor permits survival of dissociated human embryonic stem cells. Nat. Biotechnol. *25*, 681–686.

Wichterle, H., Turnbull, D.H., Nery, S., Fishell, G., and Alvarez-Buylla, A. (2001). In utero fate mapping reveals distinct migratory pathways and fates of neurons born in the mammalian basal forebrain. Development *128*, 3759–3771.

Zaitsev, A.V., Povysheva, N.V., Gonzalez-Burgos, G., Rotaru, D., Fish, K.N., Krimer, L.S., and Lewis, D.A. (2009). Interneuron diversity in layers 2-3 of monkey prefrontal cortex. Cereb. Cortex *19*, 1597–1615.

Zhao, Y., Flandin, P., Long, J.E., Cuesta, M.D., Westphal, H., and Rubenstein, J.L. (2008). Distinct molecular pathways for development of telencephalic interneuron subtypes revealed through analysis of Lhx6 mutants. J. Comp. Neurol. *510*, 79–99.